Available online at www.sciencedirect.com
SCIENCE DIRECT®
Journal of Solid State Chemistry 178 (2005) 2527–2532
JOURNAL OF SOLID STATE CHEMISTRY
www.elsevier.com/locate/jssc

Gas sorption properties of microporous metal organic frameworks

JeongYong Lee[a], Jing Li[a,*], Jacek Jagiello[b]

[a]*Department of Chemistry and Chemical Biology, Rutgers University, The State University of New Jersey, Wright-Rieman Laboratories, 610 Taylor Road, Piscataway, NJ 08854, USA*

[b]*Quantachrome Instruments, 1900 Corporate Drive, Boynton Beach, FL 33426, USA*

Received 30 April 2005; received in revised form 9 June 2005; accepted 5 July 2005

Abstract

A low-temperature gas sorption study has been carried out on four three-dimensional microporous metal organic framework (MMOF) structures and two two-dimensional layered structures. The pore characteristics are analyzed based on the argon adsorption–desorption isotherms at 87 K. The results from hydrogen sorption experiments conducted at 77 and 87 K show that all MMOFs have a relatively high hydrogen uptake, with adsorbed hydrogen densities falling in the range of liquid hydrogen. Isosteric heats of hydrogen adsorption data calculated based on the Clausius–Clapeyron equation are consistent with these observations, indicating strong sorbent–sorbate interactions.

Keywords: Hydrogen adsorption; Gas sorption; Isostereic heat of adsorption; Metal organic framework

1. Introduction

There has been an increasing interest in the exploitation of porous materials for possible applications in the area of on-board hydrogen storage. Research in this area is highly challenging due to the fact that hydrogen has a very low gravimetric and volumetric density. Thus, all existing hydrogen storage methods, including compressed gas, liquefaction, metal hydrides and porous carbon-based adsorbents, have various difficulties that must be overcome before large-scale commercialization can be considered [1]. Developing new storage materials that significantly increase hydrogen storage capability also becomes imperative. Some very recent work has spotlighted a new type of metal-organic-based materials as promising candidates [2]. Metal organic frameworks (MOFs) are a general family of one-dimensional (1D), two-dimensional (2D) or three-dimensional (3D) metal coordination network structures consisting of metals and organic linkers, for example a dicarboxylic acid and/or a pyridine derivative. A sub-group of MOFs that contain pores with dimensions less than 2 nm is designated as microporous metal organic frameworks or MMOFs. The key features of these porous materials are well-characterized pores, small pore dimension, high micropore volume, and high surface area. The pore size, shape, and structure of MMOFs can often be modified to enhance sorbate–sorbent interactions. These advantageous properties make them attractive for potential applications such as gas separation and catalysis [3–5], sensing devices [6,7], ion exchange [8,9] and optoelectronics [10,11]. Recent studies show very interesting hydrogen sorption properties in several MMOFs [12–16].

In this paper, we present gas sorption properties of several MMOFs. These are 3D $[Zn_3(bpdc)_3bpy]\cdot 4DMF\cdot H_2O$ (**1**) (bpdc = biphenyldicarboxylate, bpy = 4,4′-bipyridine, DMF = *N*,*N*-dimethylformamide) and $[Co_3(bpdc)_3bpy]\cdot 4DMF\cdot H_2O$ (**2**); 3D Cu-(hfipbb)$(H_2hfipbb)_{0.5}$ (**3**) (H_2hfipbb = 4,4-(hexafluoroisopropylidene)-bis(benzoic acid); and 3D $Cu_3(BTC)_2(H_2O)_3$ (**4**) (BTC = benzene-1,3,5-tricarboxylate), all having 1D open channels. For comparison purposes, we also report

*Corresponding author. Fax: +732 445 5312
E-mail address: jingli@rutchem.rutgers.edu (J. Li).

0022-4596/$ - see front matter © 2005 Elsevier Inc. All rights reserved.
doi:10.1016/j.jssc.2005.07.002

sorption properties of two 2D layered structures, Co(ox)(bpy) (**5**) (ox = $C_2O_4^{2-}$) and Ni(ox)(bpy) (**6**) that do not contain any open channels.

2. Experimental section

2.1. Preparation of 3D $Zn_3(bpdc)_3bpy]\cdot 4DMF\cdot H_2O$ (*1*) and $Co_3(bpdc)_3bpy]\cdot 4DMF\cdot H_2O$ (*2*)

Both **1** and **2** were prepared via reactions described in our earlier work [16,17]. $Zn(NO_3)_2\cdot 6H_2O$ (98%,Acros), $Co(NO_3)_2\cdot 6H_2O$ (99%,Acros), bpdc (Aldrich, 99% +), bpy (Acros, 98%), and DMF (Fischer, 99% + Reagent Grade) were used as received without further purification. Column-like colorless crystals of $[Zn_3(bpdc)_3bpy]\cdot 4DMF\cdot H_2O$(**1**) were obtained by reaction of $Zn(NO_3)_2\cdot 6H_2O$ (0.059 g) with bpdc (0.048 g) and bpy (0.031 g) in 10 mL of DMF solution in the molar ratio of 1:1:1:0.65 at 150 °C for 48 h. Reactants were mixed in a Teflon-lined autoclave and heated in an oven at a constant temperature. After the reaction, the autoclave was cooled naturally to room temperature. The solution was filtered and the product was washed with DMF (10 mL × 3 times) and the crystals were dried at 80 °C for 3 h. The purple-colored column shaped crystals of **2** were grown in a reaction of $Co(NO_3)_2\cdot 6H_2O$ (0.020 g) with bpdc (0.025 g) and bpy (0.016 g) in DMF (5 mL) at 150 °C for 48 h. The same filtering and drying conditions of **1** were applied to **2**.

2.2. Preparation of 3D $[Cu\text{-}(hfipbb)(H_2hfipbb)_{0.5}]$ (*3*)

$Cu(NO_3)_2\cdot 3H_2O$ (99%, Acros) and H_2hfipbb (Aldrich, 99%) were used as received without further purification. Column-shaped blue crystals of **3** were synthesized by a hydrothermal reaction of $Cu(NO_3)_2\cdot 3H_2O$ (0.024 g, 0.1 mmol) with excess H_2hfipbb (0.122 g, 0.31 mmol) in 5 mL of deionized water at 150 °C for 12 h [12]. The molar ratio of the reaction was 1:3.1:2778. Excess H_2hfipbb was removed by repeatedly washing the product with 10 mL of DMF, followed by drying the product in air for an hour.

2.3. Preparation of 3D $[Cu_3(BTC)_2(H_2O)_3]$ (*4*)

$Cu(NO_3)_2\cdot 3H_2O$ (98%, Aldrich) and trimesic acid or BTC (Aldrich, 95%) were used as received without further purification. Blue crystals of **4** were obtained from a reaction of $Cu(NO_3)_2\cdot 3H_2O$(0.435 g, 1.8 mmol) dissolved in 6 mL of de-ionized water with trimesic acid (0.110 g, 0.5 mmol) dissolved in 6 mL of ethanol. The solution was then transferred into a Teflon-lined autoclave and heated in an oven at 403 K for 12 h. Chui et al. [18] reported crystal growth of **4** at 453 K under hydrothermal conditions which also generated a by-product Cu_2O. Several others reported preparation of the same compound at lower temperatures [19,20]. A simulation study of Ar adsorption in **4** was carried out by Skoulidas [21].

2.4. Preparation of 2D $[Co(ox)(bpy)]$ (*5*) and $[Ni(ox)(bpy)]$ (*6*)

$CoCl_2$ (Alfa Aesar, 99 + %), $NiCl_2$ (Alfa Aesar, 99 + %), bpy (Acros, 98%), and $Na_2C_2O_4$ (Alfa Aesar, 99%) were used as received without further purification. Coral plate crystals of **5** were prepared by a hydrothermal reaction of $CoCl_2$ (0.1297 g), bpy (0.1562 g), sodium oxalate (0.1340 g), and H_2O (8 mL) in the molar ratio of 1:1:1:444 at 170 °C for 4 days [22]. Light blue plate crystals of **6** were grown from a hydrothermal reaction containing $NiCl_2$ (0.1296 g), bpy (0.1562 g), sodium oxalate (0.1340 g), and H_2O (8 mL) in the molar ratio of 1:1:1:444. Under identical experimental conditions the reactions generated single-phased polycrystalline compounds of **5** and **6**.

2.5. Gas sorption measurements

The gas adsorption–desorption experiments were conducted using an automated micropore gas analyzer Autosorb-1 MP (Quantachrome Instruments). The cryogenic temperatures were controlled using liquid argon and liquid nitrogen at 87 and 77 K, respectively. The initial outgassing process for each sample was carried out under vacuum at 373 K for 6–8 h. About 0.05–0.08 g of samples were used for gas sorption studies and the weight of each sample was recorded before and after outgassing to confirm of the removal of guest molecules. The outgassing procedure was repeated on the same sample between experiments for 0.5–1 h. A total analysis time were ca. 60–130 h for Ar sorption and 7–9 h for hydrogen sorption. Pore properties including pore volume, pore size, and surface area were analyzed using Autosorb v1.50 software.

3. Results and discussion

3.1. Gas sorprion of $[Zn_3(bpdc)_3bpy]\cdot 4DMF\cdot H_2O$ (*1*) and $[Co_3(bpdc)_3bpy]\cdot 4DMF\cdot H_2O$ (*2*)

3.1.1. Ar sorption at 87 K

The 3D channel structures of **1** and **2** are shown in Fig. 1a and b, respectively. The purity of both polycrystalline samples was confirmed by PXRD and their thermal stability was validated by thermogravimetric (TG) analysis. Both compounds clearly showed a two-stage weight loss at ~200 and ~400 °C. The weight loss around 200 °C was 21% for **1** and 22% for **2**, in agreement with the calculated amount of guest

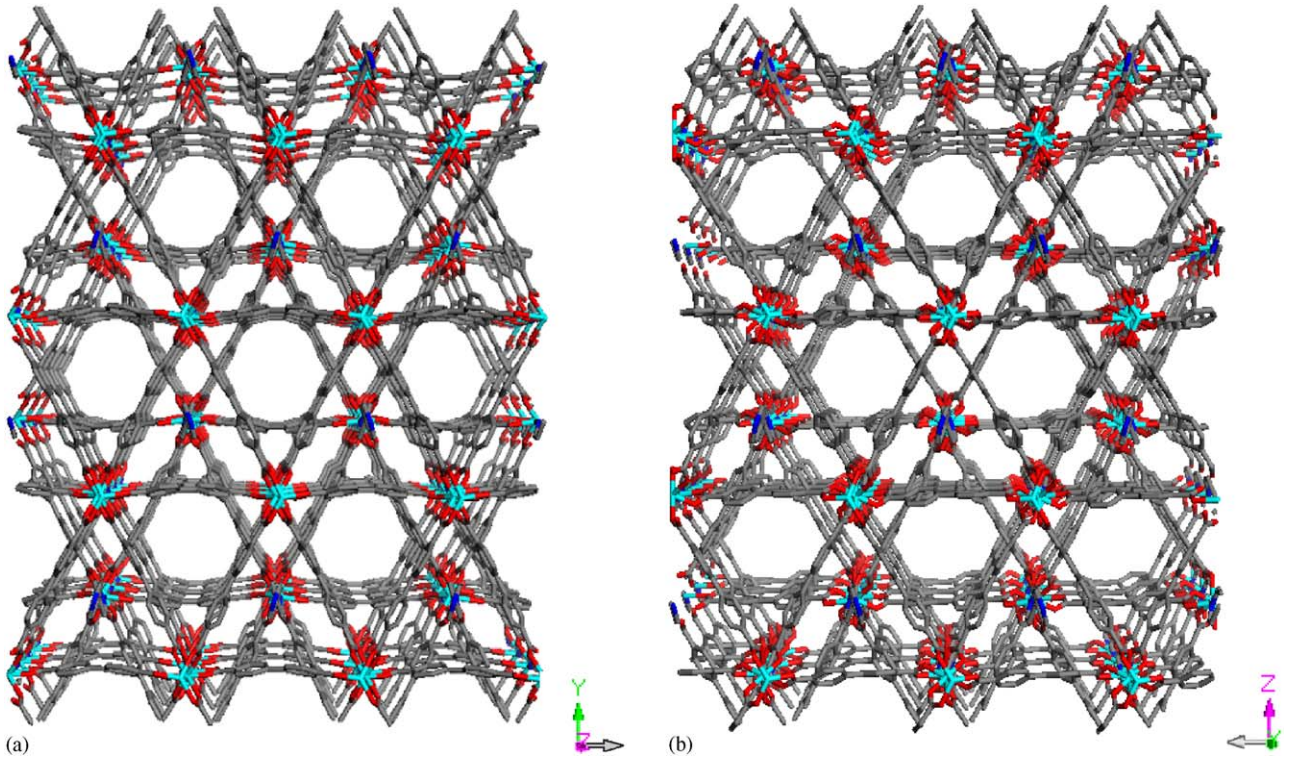

Fig. 1. (a) The three-dimensional (3D) channel structure of $[Zn_3(bpdc)_3bpy]\cdot 4DMF\cdot H_2O$ (**1**) and (b) that of $[Co_3(bpdc)_3bpy]\cdot 4DMF\cdot H_2O$ (**2**) . In the figure, Zn and Co are shown in cyan, O is shown in red, N is shown in blue, C is shown in gray and H is omitted for clarity.

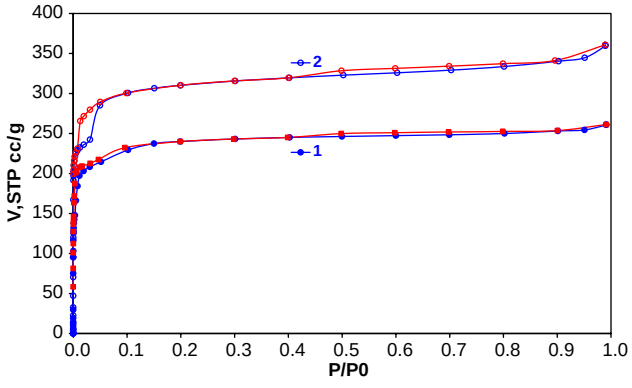

Fig. 2. The Ar adsorption (blue) and desorption (red) isotherms on $[Zn_3(bpdc)_3bpy]\cdot 4DMF\cdot H_2O$ (**1**) and $[Co_3(bpdc)_3bpy]\cdot 4DMF\cdot H_2O$ (**2**) obtained at 87 K.

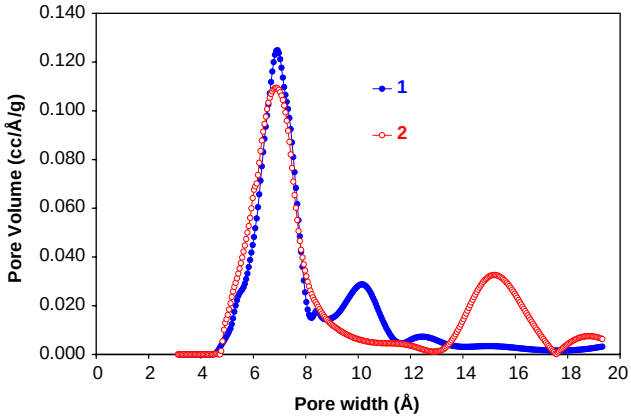

Fig. 3. Pore size distribution of $[Zn_3(bpdc)_3bpy]\cdot 4DMF\cdot H_2O$ (**1**) and $[Co_3(bpdc)_3bpy]\cdot 4DMF\cdot H_2O$ (**2**) calculated from the Horvath–Kawazoe (H–K) model.

molecules (DMF and H_2O). The decomposition of **1** and **2** occurred at 384 and 400 °C, respectively, which was confirmed by the PXRD analysis. The Ar adsorption–desorption isotherms of both compounds are depicted in Fig. 2. Both compounds showed a tiny hysteresis at $P>0.4$ atm which is typically a result of intercrystalline voids in the samples [20]. Both compounds also exhibited a rather large low-pressure hysteresis at $P<0.05$ for **2** and $P<0.05$ for **1**, with that in **2** much more significant. This is believed to originate from the change in volume of the adsorbent [23a,b]. Depicted in Fig. 3 is pore size distribution based on Horvath–Kawazoe (H–K) model [24]. This analysis shows that two types of pores exist in **1**. A large portion of these pores have a pore diameter less than 7 Å which falls in the range of ultramicropores (pore diameter <7 Å). A small portion of the pores has a pore diameter about 10 Å, falling in the range of supermicropores (pore diameter within 7–20 Å). These data are consistent with the dimensions estimated based on the single crystal structure of **1**. Similarly, the H–K model gives two types of pores for **2**: ultramicropores (diameters ~7 Å) and supermicropores (diameters ~15 Å) [23b].

While we expect a small difference in their supermicropore dimension because of the difference in the channel structures of **1** and **2**, where the 6-membered rings consisting of the internal wall of the 1D channels in **1** rotate somewhat more into the channels than **2** does, so that the channels in **1** have more atoms "sticking into the void", resulting in a reduced pore dimension, the pore diameter of 15 Å from the H–K model is significantly larger than what was estimated from the crystal structure of **2**. The total pore volume estimated based on their Ar isotherm data is consistent with these observations, giving a value of 0.33 cc/g for **1** and 0.38 cc/g for **2**.

3.2. Gas sorption of 3D [Cu-(hfipbb)(H_2hfipbb)$_{0.5}$] (3)

In general, small pores having dimensions comparable to molecular hydrogen diameter are important for high magnitude of hydrogen adsorption. We measured hydrogen adsorption–desorption isotherms on Cu-(hfipbb)(H_2hfipbb)$_{0.5}$ (**3**) that contains ultramicrochannels, that is, channels with pore diameters falling in the range of ultramicropores. The crystal structure of **3** is shown in Fig. 4. The ultramicrochannels are formed by alternating smaller windows and larger cages. The dimensions of the small windows are $\sim 3.5 \times 3.5$ Å (calculated based on the van der Waals radius of carbon), and the dimensions of the larger cages are $\sim 5.1 \times 5.1$ Å. Low pressure high-resolution hydrogen sorption measurements can provide useful information on gas–solid interactions between adsorbate and adsorbent. The hydrogen adsorption–desorption isotherms were measured on **3** at two cryogenic temperatures, 77 and 87 K, and the results are plotted in Fig. 5. Strong hysteresis was observed at all pressure levels, and the extent increases as the temperature increases, as showed in Fig. 5. This behavior is very different from that of **1** and **2**, most likely a result of much smaller pore dimensions in **3** [16a]. The maximum values of hydrogen uptake are 0.21 wt% at 87 K (1 atm) and 0.23 wt% at 77 K (1 atm), Note the density of adsorbed hydrogen at these temperatures is ~0.03–0.033 g/cc, calculated based on the estimated pore volume, 0.07 cc/g [17]. This value is the same as that of H_2 at critical point (33 K and 13 atm).

3.3. Gas sorption of [$Cu_3(BTC)_2(H_2O)_3$] (4)

The crystal structure of [Cu_3(BTC)$_2$(H_2O)$_3$] (**4**) is shown in Fig. 6. Although sorption properties for N_2,

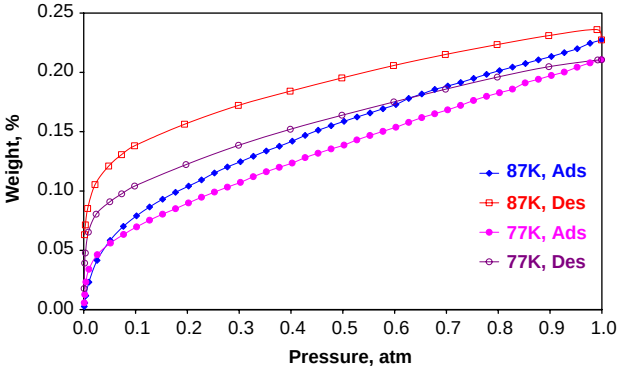

Fig. 5. The hydrogen adsorption–desorption isotherms on Cu-(hfipbb)(H_2hfipbb)$_{0.5}$ (**3**) at 77 and 87 K.

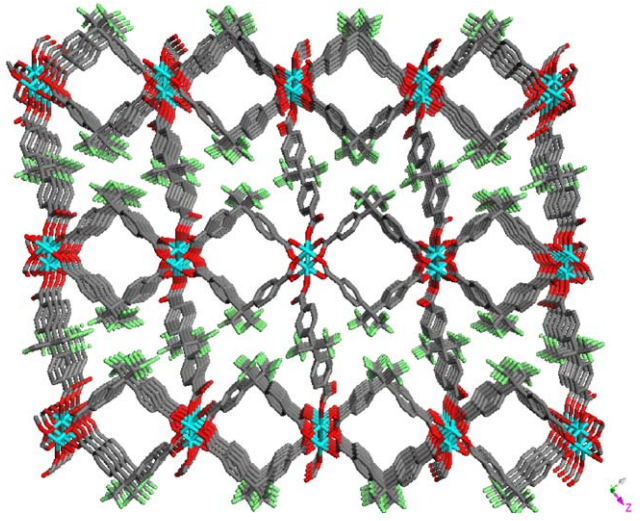

Fig. 4. The three-dimensional (3D) ultramicrochannel structure of Cu-(hfipbb)(H_2hfipbb)$_{0.5}$ (**3**). In the figure, Cu is shown in cyan, F is shown in green, O is shown in red, C is shown in gray and H is omitted for clarity.

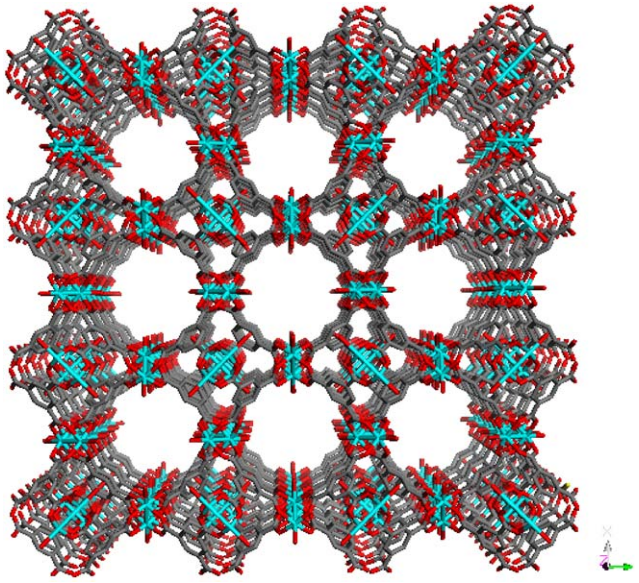

Fig. 6. The crystal structure of Cu_3(BTC)$_2$(H_2O)$_3$ (**4**). In the figure, Cu is shown in cyan, O is shown in red, C is shown in gray and H is omitted for clarity.

O_2, CO, CO_2, N_2O, CH_4, ethylene, ethane, *n*-dodecane, as well as water have been reported previously [3], hydrogen sorption study has not been conducted to this date. Here, we performed both argon and hydrogen sorption experiments on **4**. The Ar isotherms of **4** were obtained at 87 K at pressures ranging from $p<10^{-6}$ to 1 atm. The results are shown in Fig. 7. Two steps are observed in the Ar sorption isotherm, a result of two types of pores: central channels and outside pockets as claimed by Vishnyakov et al. [20]. The pore volume was estimated to be 0.40 cc/g. The hydrogen uptakes of **4** are 1.07 wt% at 87 K, 1 atm and 1.44 wt % at 77 K, 1 atm, as depictured in Fig. 8. The adsorbed hydrogen density is 0.036 g/cc, within the range of liquid hydrogen density, 0.03–0.076 g/cc [25]. The pore size distribution data obtained using the H–K method [24] confirm that there are two different pores, the ultramicropores having diameters of ~6 Å and supermicropores of ~8 Å in diameters. The extent of gas–solid interactions can be assessed using isosteric heat of adsorption, Q_{st}, which is based on the Clausius–Clapeyron equation [26,27]. The calculated isosteric heats of hydrogen adsorption of **4** are shown in Fig. 9. The Q_{st} values are in the range of 6–7 kJ/mol, significantly higher than the enthalpy of vaporization of H_2 (0.99 kJ/mol at its boiling point). They are also similar to those calculated for compounds **1** and **2**, indicative of a strong hydrogen–adsorbent interaction within the pores [16a].

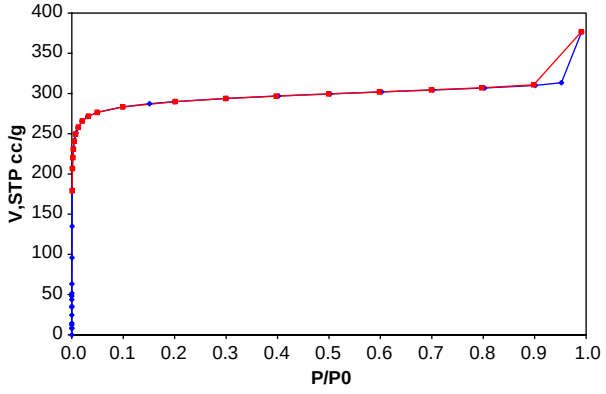

Fig. 7. The Ar adsorption (blue)–desorption (red) isotherms of **4** at 87 K.

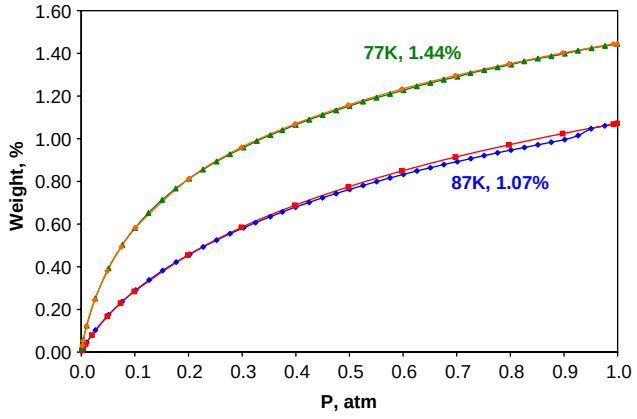

Fig. 8. The H_2 adsorption–desorption isotherms for **4** at 87 and 77 K (blue and green lines are adsorption, red and orange lines are desorption).

3.4. *Gas sorprion of 2D [Co(ox)(bpy)] (5) and [Ni(ox)(bpy)] (6)*

The 2D structures of [Co(ox)(bpy)] (**5**) and [Ni(ox)(bpy)] (**6**) are shown in Fig. 10a. Both structures contain octahedrally coordinated metal centers bonded to two oxalate and two bpy ligands to form a 2D layered network with an interlayer distance of 5.3–5.5 Å [22]. Different from 3D structures **1**–**4**, compound **5** and **6** demonstrate very low sorption capability. The hydrogen uptakes at 77 K, 0.10 wt% for **5** and 0.16 wt% for **6**, respectively, are significantly lower compared to those of **1**–**4**. The hydrogen adsorption–desorption isotherms measured at 77 K are shown in Fig. 10b, along with those of **4**. Note that both **5** and **6** exhibit strong hysteresis in their adsorption–desorption isotherms.

4. Concluding remarks

The sorption properties of four 3D MMOFs (**1**–**4**) and two 2D layered structures have been investigated at 87 and 77 K. Analysis of their pore characterizations has been made based on these data. All MMOFs exhibit a relatively high hydrogen uptake, with adsorbed hydrogen densities comparable to that of liquid hydrogen. This is also confirmed by isosteric heats of hydrogen adsorption data, calculated based on the Clausius–Clapeyron equation.

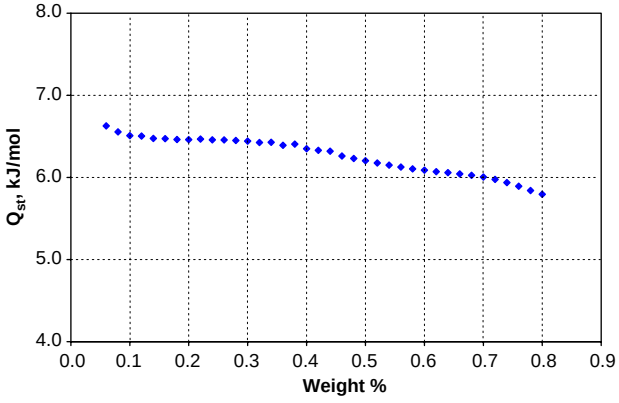

Fig. 9. The isosteric heat of hydrogen adsorption (Q_{st}) for **4** as a function of the amount of hydrogen adsorbed.

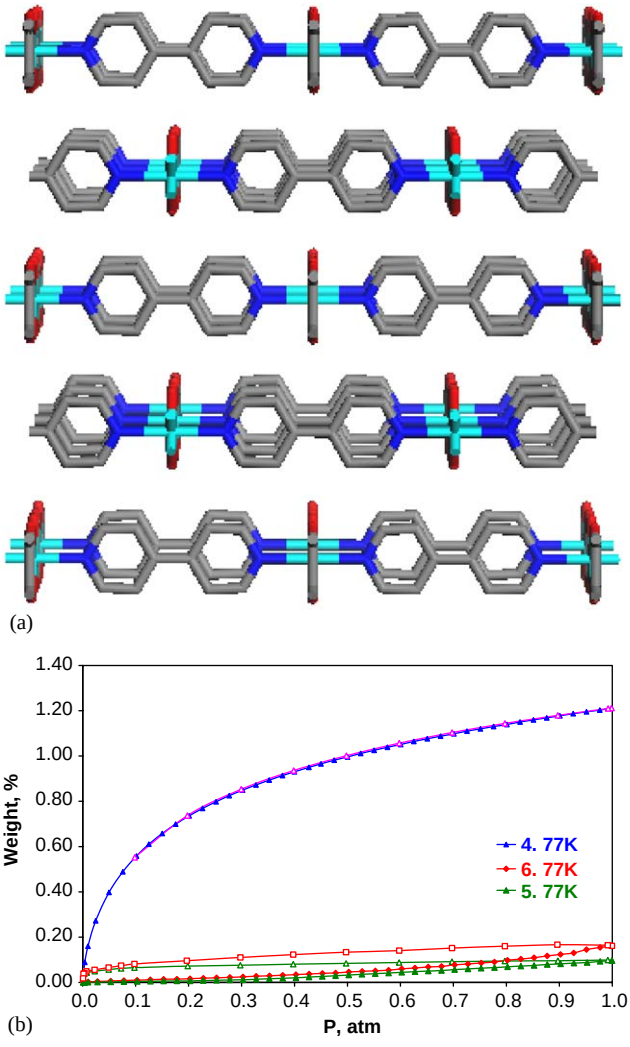

Fig. 10. (a) The crystal structures of [Co(ox)(bpy)] (**5**) and [Ni(ox)(bpy)] (**6**). (b) The H_2 adsorption–desorption isotherms for **5** and **6** at 77 K, compared with those of **4**. Solid marks are for adsorption and open marks are for desorption.

Acknowledgments

We acknowledge the donors of The Petroleum Research Fund, administrated by the ACS, for supporting this research. The authors also acknowledge partial support from the National Science Foundation (Grant No. DMR-0422932). We thank Xiaoying Huang for structure analysis and Dr. Long Pan for helpful discussions.

References

[1] Fuel Cells, and Infrastructure Technologies Program, US DOE, November 2002 (http://www.eere.energy.gov/hydrogenandfuelcells/pdfs/33098_toc.pdf).
[2] N.L. Rosi, J. Eckert, M. Eddaoudi, D.T. Vodak, J. Kim, M. O'Keeffe, O.M. Yaghi, Science 300 (2003) 1127.
[3] Q.M. Wang, D.M. Shen, M. Bülow, M.L. Lau, S.G. Deng, F.R. Fitch, N.O. Lemcoff, J. Semanscin, Micropor. Mesopor. Mater. 55 (2002) 217.
[4] J. Seo, D. Whang, H. Lee, S. Jun, J. Oh, Y. Jeon, K. Kim, Nature 404 (2000) 982.
[5] T. Sawaki, Y. Aoyama, J. Am. Chem. Soc. 121 (1999) 4793.
[6] M. Albrecht, M. Lutz, A.L. Spek, G. Koten, Nature 406 (2000) 970.
[7] L.G. Beauvais, M.P. Shores, J.R. Long, J. Am. Chem. Soc. 122 (2000) 2763.
[8] K. Min, M. Suh, J. Am. Chem. Soc. 122 (2000) 6834.
[9] O.M. Yaghi, H. Li, J. Am. Chem. Soc. 118 (1996) 295.
[10] O.R. Evans, W. Lin, Chem. Mater. 13 (2001) 2705.
[11] Y. Dong, G. Jin, M. Smith, R. Huang, B. Tang, H.-C. zur Loye, Inorg. Chem. 41 (2002) 4909.
[12] L. Pan, M.B. Sander, X. Huang, J. Li, M. Smith, E. Bittner, B. Bockrath, J.K. Johnson, J. Am. Chem. Soc. 126 (2004) 1308.
[13] D.N. Dybtsev, H. Chun, S. Yoon, D. Kim, K. Kim, J. Am. Chem. Soc. 126 (2004) 32.
[14] E.Y. Lee, M.P. Suh, Angew. Chem. Int. Ed. 43 (2004) 2798.
[15] J.C. Rowsell, A.R. Millward, K. Park, O.M. Yaghi, J. Am. Chem. Soc. 206 (2004) 5666.
[16] (a) J.Y. Lee, L. Pan, S.P. Kelly, J. Jagiello, T.J. Emge, J. Li, Adv. Mater. (2005), in press;
(b) L. Pan, H.-M. Liu, X. Lei, X. Huang, D.H. Olson, N.J. Turro, J. Li, Angew. Chem. Int. Ed. 42 (2003) 542.
[17] L. Pan, M.B. Sander, X.-Y. Huang, D.H. Olson, J. Li, Angew. Chem., manuscript submitted.
[18] S. Chui, S. Lo, J. Charmant, A.G. Orpen, I.D. Williams, Science 283 (1999) 1148.
[19] K. Schlichte, T. Kratzke, S. Kaskel, Micropor. Mesopor. Mater. 73 (2004) 81.
[20] A. Vishnyakov, P.I. Ravikovitch, A.V. Neimark, M. Bulow, Q.M. Wang, Nano Letters 3 (2003) 713.
[21] A.I. Skoulidas, J. Am. Chem. Soc. 126 (2004) 1356.
[22] J.Y. Lu, M.A. Lawandy, J. Li, T. Yuen, C.L. Lin, Inorg. Chem. 38 (1999) 2695.
[23] (a) S. Lowell, J.E. Shields, M.A. Thomas, M. Thommes, Characterization of Porous Solids and Powders: Surface Area, Pore Size, and Density, Kluwer Academic Publishers, July 2004 (Chapter 4);
(b) K.S.W. Sing, D.H. Everett, R.A.W. Haul, L. Moscou, R.A. Pierotti, J. Rouquerol, T. Siemieniewska, Pure Appl. Chem. 57 (1985) 603.
[24] G. Horvath, K. Kawazoe, J. Chem. Eng. Jpn. 16 (5) (1983) 470.
[25] http://www.nist.gov/.
[26] D. Shen, M. Bülow, Adsorption 6 (2000) 275.
[27] A. Anson, M.A. Callejas, A.M. Benito, W.K. Maser, M.T. Izquierdo, B. Rubio, J. Jagiello, M. Thommes, J.B. Parra C., M.T. Martınez, Carbon 42 (2004) 1243.